21st Australasian Fluid Mechanics Conference
Adelaide, Australia
10-13 December 2018

Ultrafine Particle Transport and Deposition in the Upper Airways of a CT-Based Realistic Lung

S. C. Saha[1] and Mohammad S. Islam[1]

[1]School of Mechanical and Mechatronics Engineering
University of Technology Sydney, Sydney, NSW-2007, Australia

Abstract

The understanding of the toxic pollutant particles transport and deposition is important for dosimetry and respiratory health effects analysis. The studies over the last few decades for ultrafine particle transport and deposition improves the understanding of the drug-aerosol impacts in the extrathoracic airways. A limited number of studies has also considered upper airways and almost all of those studies used the non-realistic smooth surface for upper airway model. However, the smooth surface anatomical model is far from the realistic lung and it is important to consider realistic lung model for better prediction of ultrafine particle deposition. This study aims to simulate the ultrafine particle transport and deposition in the upper airways of a highly asymmetric CT-based model. The anatomically explicit digital airway model is generated from the high-resolution CT data of a healthy adult. Unstructured tetrahedral mesh throughout the geometry and fine inflation layer mesh near the wall is generated. Euler-Lagrange (E-L) approach and ANSYS Fluent solver (18.2) are used to investigate the ultrafine particle transport and deposition. A wide range of diameter ($1 \leq$ nm ≤ 1000) and different flow rates are considered for the ultrafine particle simulation. Pressure drop is calculated for right and left lobes which might be helpful for the therapeutic purpose of the asthma patient. The numerical study shows that the deposition efficiency in the right lung and the left lung is different for dissimilar flow rates, which could help the health risk assessment of the respiratory diseases and eventually could help the targeted drug delivery system.

Themes: Computational fluid dynamics, Multiphase and particle-laden flows, Biomedical fluid mechanics, Micro/biofluid mechanics.

Introduction

Different natural and man-made sources emit a significant amount of nano-sized particles into the atmosphere. The particles exposed due to combustion and nucleation may grow by condensation of the gas clusters, or coagulation with other atmospheric particulates. Cosmic and weather dependent phenomenon such as hurricanes, volcanic eruptions also produces ultrafine particle to the atmosphere. Incomplete biomass burning produces polycyclic aromatic hydrocarbons (PAH) which is generally carcinogenic substance and compound of more than 100 different chemicals ([1, 2]). The pollutant PAH can be in different forms (volatile, semi-volatile) and they may combine with the pollutant nanoparticle at the atmosphere. For this reason, nanoparticles can be more pollutant than the micro-particles and may contribute to severe respiratory diseases. Due to the smaller size, the atmospheric nanoparticles can enter, penetrate, translocate and damage the living organisms of the human lung [3]. Therefore, the knowledge of the nanoparticle deposition at the human respiratory airways is important for an appropriate health risk assessment. A number of studies have reported the nanoparticle transport and deposition (TD) in the nasopharyngeal region of the lung ([4-8]). There are fewer number of studies that have been conducted for nanoparticle TD in the tracheobronchial and deeper airways. The complexity of the nanoparticle generation in the experimental study, the difficulty of defining an accurate drug law and the individual correction factor for specific nanoparticles in a CFD study are the major difficulties for nanoparticle TD prediction. There are limited number of studies available dealing with nanoparticle TD in the tracheobronchial airways of the human lung. A series of studies ([9-11]) have calculated the mass transfer and deposition in the upper airways. An experimental study of a human cast reported ultrafine particle deposition and compared it with analytical data ([12]). The study concludes that the deposition density at the bifurcation area is 20% greater than the airway length. Zhang and Kleinstreuer [13] performed the airflow structure and nanoparticle deposition for a triple bifurcation model. The Euler-Euler (E-E) approach reports that the turbulence effects on nanoparticle deposition are negligible. The E-E approach is found computationally suitable for a large number of particles. On contrary, E-L approach considers particle diffusivity, inertia, electrostatic effects and near wall conditions to track the individual particles [14]. This study considered E-L approach to investigate the different diameter particles TD in the upper airways. Ultrafine particle TD is quite complicated due to its tiny size and the deposition pattern depends on different physical conditions. An explicit understanding of the ultrafine particles transport and deposition in the realistic upper airways during different physical conditions are important for better respiratory hazard assessment. To the best of authors' knowledge there are no CFD studies performed to investigate the ultrafine particle TD in the CT-based upper airways for resting condition.

Geometry Generation

A realistic bifurcation model is generated from the high-resolution CT images of a 51 years healthy adult man. The visualization software AMIRA and Geomagic are used to visualize the CT-images and surface rendering respectively. The constructed 3-D model is imported to SolidWorks for further post-processing. Figure 1 shows the visualization of the CT images and constructed 3D model of the tracheobronchial airways. The present study considers only the first three generations of the upper airways.

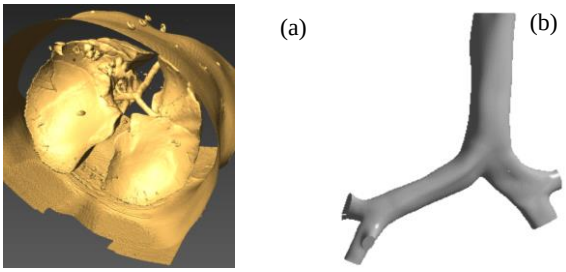

Figure 1: Realistic 3D anatomical model from CT-DiCom images; (a) 3-D model visualization from CT-Scan data and (b) Final 3D lung model.

Methods

The reconstructed conduit airway model consists of the first three generations. An advanced meshing technique is used to generate the mesh. The unstructured tetrahedral elements are used for the complex anatomical model (Figure 2). A fine inflation layer mesh is generated near the wall and dense tetrahedral element are used at the carinal angle area. High smoothing techniques are used and the minimum size of the mesh is 0.000000100252m. The mesh sensitivity analysis is performed for different sets of mesh and the final mesh contains about 3.44 million cells. ANSYS 19 solver is used for the numerical calculations of the present study. Euler-Lagrangian based Discrete Phase Model (DPM) is considered to calculate the ultrafine particle transport and deposition in the upper airways. The air is considered as the primary phase and the particle is the secondary phase in DPM. For the primary phase, the mass (1) and the momentum equations (2) are solved.

$$\frac{\partial \rho}{\partial t} + \nabla \cdot (\rho \vec{v}) = S_m \tag{1}$$

where S_m is the mass source term.

$$\frac{\partial}{\partial t}(\rho \vec{v}) + \nabla \cdot (\rho \vec{v}\vec{v}) = -\nabla p + \nabla \cdot \left(\mu \left[\left(\nabla \vec{v} + \nabla \vec{v}^T \right) - \frac{2}{3} \nabla \cdot \vec{v} I \right] \right) + \rho \vec{g} + \vec{F} \tag{2}$$

where p is fluid static pressure, $\rho \vec{g}$ is body force due to gravity, and $\vec{F}$ is body force due to external (particle-fluid interaction) force. Pressure based type solver and steady simulation are performed for the ultrafine particle TD. Viscous laminar model is used for the present study as the calculated Reynolds number for the resting condition (9lpm flow rate) is 727. SIMPLE coupling technique for pressure-velocity coupling is used to solve the DPM particle movement. A parabolic inlet condition [15] is used as below

$$u(r) = 2u_{av}(1 - \frac{r^2}{R^2}) \tag{3}$$

where R is the pipe radius.

DPM and Brownian motion are considered for ultrafine particle TD. The appropriate equation [16] is solved to investigate the individual ultrafine particles TD.

$$\frac{du_i^p}{dt} = F_D(u_i^g - u_i^p) + F_{Brownian} + F_{Lift} + \frac{\rho_p - \rho_g}{\rho_p} g_i$$
$$F_D = \frac{18\mu_g}{\rho_p d_p^2 C_c} \tag{4}$$
$$C_c = 1 + \frac{2\lambda}{d_p}(1.257 + 0.4e^{-1.1 d_p / 2\lambda})$$

where F_D is the drag force per unit particle mass, Re_p is the particle Reynolds number, and C_c is the Cunningham correction factor. The Brownian force amplitude is defined as

$$F_{Brownian} = \zeta \sqrt{\frac{\pi S_0}{\Delta t}} \tag{5}$$

where ζ is the unit variance independent Gaussian random number, Δt is the particle time-step integration. The spectral intensity (S_0) by a Gaussian white noise random process is defined as

$$S_o = \frac{216 \mu k_B T}{\pi^2 \rho_p d_p^5 (\frac{\rho_p}{\rho_g})^2 C_c} \tag{6}$$

T is the fluid absolute temperature, k_B is the Boltzmann constant, ρ_g is the gas density.
The Saffman's lift force is used (see [17]), which is a generalization of the Saffman expression (see [18]).

$$F_{Lift} = \frac{2Kv^{1/2} \rho d_{ij}}{\rho_p d_p (d_{lk} d_{kl})^{1/4}} (\vec{u} - \vec{u}_p) \tag{7}$$

where K=2.594 and d_{ij} is the deformation tensor.

A wide range of the diameter of ultrafine particles are used and the corresponding correction values for the Cunningham correction factor is employed for different diameter particles. The particle density is used as 1100 kg/m^3 and tracking parameter length scale 0.000005 is used for the present model. A total of 10,700 particles are injected from the inlet surface of the model. The velocity inlet and outflow outlet boundary condition are used in this study. The stationary wall and no-slip shear condition are used for the airway wall. The DPM wall boundary condition is used as 'trap' and Fluent user-defined function (UDF) is used to track the individual particles.

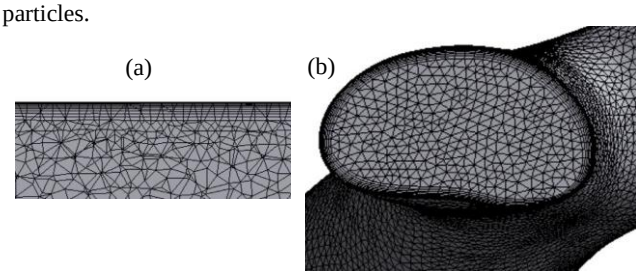

Figure 2.(a) Cross-sectional view of the inflation layer of the tracheal wall, and (b) outlet mesh at generation 3.

The numerical results are compared with the published literature for a straight pipe and a bifurcating model. The detail validation can be found in our previous study [19].

Results and Discussions

The present study accounts for nanoparticle transport and deposition of up to 3 generations of a digital airway geometry. The current study comprehensively investigated the nanoparticle transport and deposition pattern at resting condition. According to the ICRP, the flow rates 9 lpm is considered as rest-activity [20]. 1-nm, 10-nm, 50-nm, and 1000-nm diameter particles are considered in the present study.

The velocity contours at different selected planes for resting condition have been investigated. Figure 3 shows the velocity contours along with the flow vectors. The overall velocity contours at different planes show different flow patterns for resting condition. The morphological differences of the bifurcating airways, highly complex curvature at the recirculation zones, steeps and uneven airway surface influence the flow pattern at the upper airways. The randomly selected planes from the bifurcating region (plane 3, and plane 6) show the flow separation to the corresponding branches. The highly asymmetric curvature of the bifurcating airways influence the flow regime and vortex has been developed at the selected plane (plane 5) of the left lung, however, the fluid flow rate is small. The wall shear has been calculated for the realistic model at 9 lpm flow rate and found the shear rate is higher at the top of the trachea and the bifurcating bronchioles of the 2nd and 3rd generation.

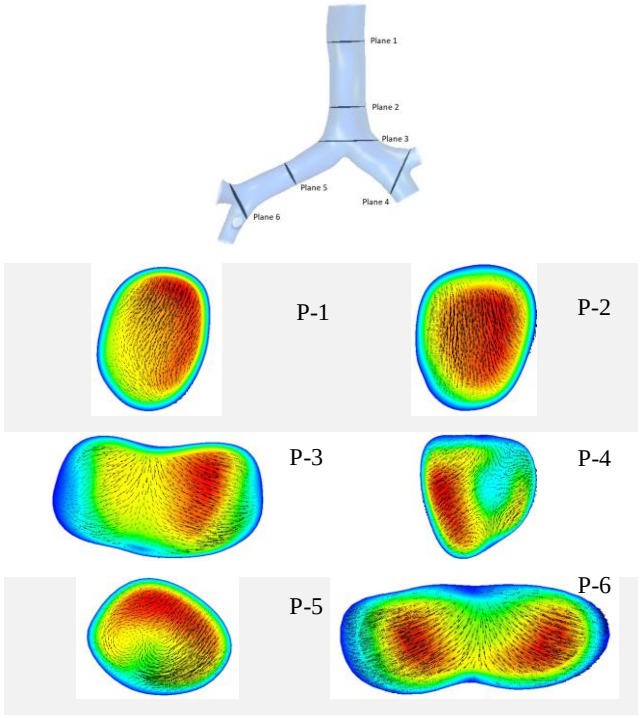

Figure 3: Velocity contour at different selected planes of the realistic geometry.

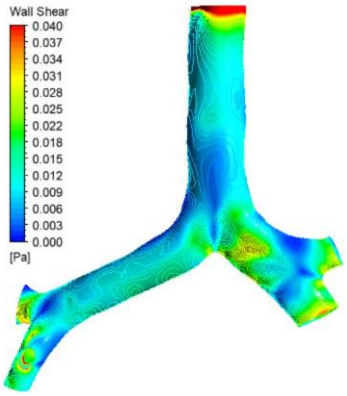

Figure 4: The wall shear at the upper airways during resting condition.

A wide range of ultrafine particles TD have been investigated for resting condition and the deposition pattern is shown in figure 5. Figures 5(a, b, c, d) show the ultrafine particle deposition scenario for 1-nm, 10-nm, 50-nm, and 100-nm diameter particle respectively. Figure 5(a) illustrates that a significant amount of 1-nm diameter particle is deposited at the tracheobronchial airways. The overall deposition pattern of 1-nm diameter particle shows a higher number of particles are deposited at the tracheal wall than the left and the right lung. Figure 5(b) shows the deposition pattern for 10-nm diameter particles. The deposition visualization of 10-nm particles depicts less deposition than the 1-nm diameter particle. The general deposition pattern shows very few numbers of particles are deposited on the right and the left lung compares to the tracheal wall. A similar deposition scenario is observed for 50-nm and 100-nm diameter particles. The overall deposition pattern for 1-nm diameter particle illustrates that Brownian diffusion is dominant for the smaller diameter particle for the upper airways. Brownian motion is the random microscopic motion of the smaller particles due to the frequent chaotic collision by gas molecules. Gas molecules collision mainly causes the diffusion, and the effectiveness of the Brownian diffusion decreases with the increase of particle diameter. The deposition pattern of the present study also supports the general hypothesis of Brownian motion. Fig. 5(d) shows only a few numbers of 100-nm particles are deposited at the bifurcating branches. With the increase of the particle diameter, the effectiveness of the Brownian diffusion decreases and the overall deposition percentage is also decreases. The inertial impaction is also not dominant for a 100-nm diameter particle as the inertia is very small. At resting condition, the flow rate is relatively small and 100-nm particle does not deviate from the air streamline due to its lower inertia. The overall deposition pattern for 50-nm and 100-nm particles reports a small number of particles are deposited at the tracheal wall and the bifurcating branches. The general deposition pattern for larger diameter nanoparticle indicates that almost all of the 50-nm and 100-nm diameter particles escaped through the outlets of the present model and those particles are supposed to travel remaining generations (4^{th}-23^{rd}).

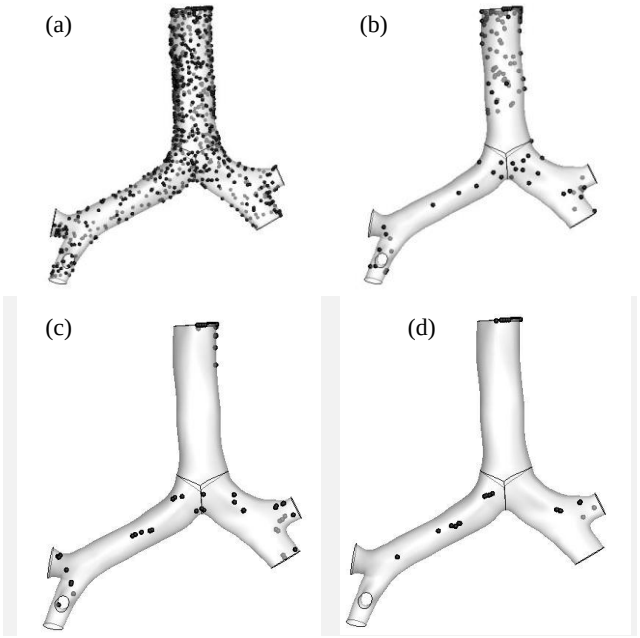

Figure 5: Ultrafine particle deposition pattern for different diameter particles at 9 lpm flow rate, (a) 1-nm, (b) 10-nm, (c) 50-nm, and (d) 100-nm.

The deposition efficiency of the different diameter nanoparticles at different parts of the lung have been investigated for resting conditions. Figure 6 shows the DE comparison at the trachea, the right lung, and the left lung. The numerical investigation reports that the nanoparticle DE is significantly higher at the tracheal wall compare to the right lung and the left lung for 1-nm diameter particles. About 6.2% of the 1-nm diameter particles are deposited at the tracheal wall. The DE comparison also reports that the DE at the left lung is higher than the right lung for 1-nm and 10-nm diameter particles. On contrary, 50-nm diameter particles DE at the right lung is higher than the left lung, however, the left lung of the present model consists higher number of branches than the right lung. The DE comparison also depicts that the DE at the tracheal wall decreases with the increase of the nanoparticles diameter and which also support the general phenomenon of nanoparticle TD.

Figure 7 shows the 1-nm, 10-nm, 50-nm and 100-nm diameter ultrafine particle deposition density at the trachea. The deposition density comparison histogram reports that the deposition density is significantly higher at the top of the trachea than the other parts

of the trachea. The histogram depicts the deposition hot spot at the different region of the trachea for different diameter particles which will help the targeted drug delivery system.

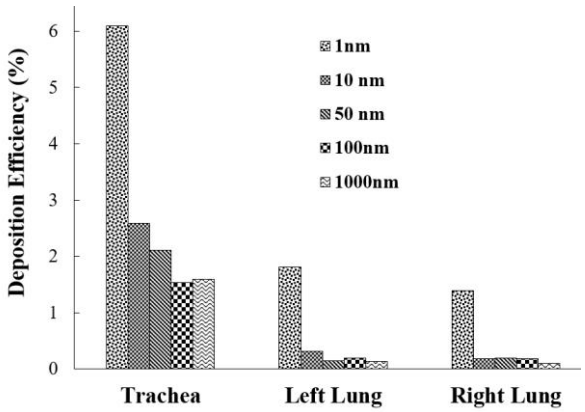

Figure 6: Ultrafine particles DE in the sleeted zones of the realistic model at 9 lpm flow rate.

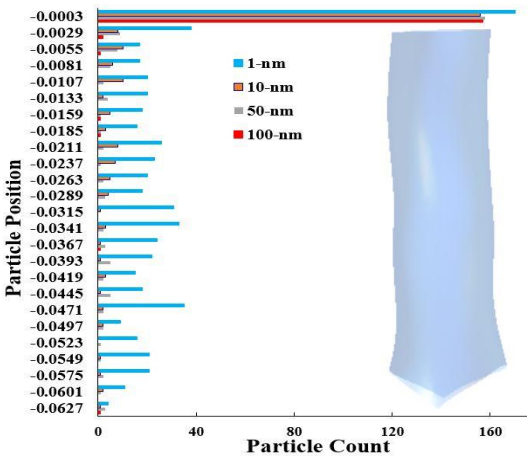

Figure 7: Ultrafine particle deposition density comparison at the trachea for different diameter particles.

Conclusions

The present CFD study investigates ultrafine particle TD in the upper airways of a CT-Scan model. This model is developed for ultrafine particle TD for resting physical condition. A MATLAB code is developed to investigate the deposition hot spot for realistic model. The conclusions of the present study is summerised as:

- Brownian motion is the principal mechanism for ultrafine particle TD. The effectiveness of the Brownian motion decreases with the increases of particle diameter. About 10 percent of 1-nm particles are deposited at the upper airways whereas, only 2 percent of 100-nm diameter particles are deposited;
- Deposition efficiency at the tracheal wall is higher than the left and the right lung;
- A higher percentage of 1-nm particles are deposited at the right lung than left lung. On contrary, a higher number of 50-nm particle is deposited at left lung than right lung.

The findings of this study will enhance the understanding of the ultrafine particles TD in the realistic lung model. The present study reveals the deposition hot spot for different diameter particles which will potentially help the targeted drug delivery system. The future study will consider a large-scale model with more detail branching airways for ultrafine particle TD.

Acknowledgment

The authors would like to thank the high-performance computing Unit ARC LAB, University of Technology Sydney, Australia.

References

1. Jenkins, B.M., et al., *Particle concentrations, gas-particle partitioning, and species intercorrelations for polycyclic aromatic hydrocarbons (PAH) emitted during biomass burning.* Atmospheric Environment, 1996. **30**(22): p. 3825-3835.
2. Chen, J., et al., *A review of biomass burning: Emissions and impacts on air quality, health and climate in China.* Science of The Total Environment, 2016.
3. Buzea, C., I.I. Pacheco, and K. Robbie, *Nanomaterials and nanoparticles: sources and toxicity.* Biointerphases, 2007. **2**(4): p. MR17-MR71.
4. Xi, J. and P.W. Longest, *Numerical predictions of submicrometer aerosol deposition in the nasal cavity using a novel drift flux approach.* International Journal of Heat and Mass Transfer, 2008. **51**(23): p. 5562-5577.
5. Inthavong, K., K. Zhang, and J. Tu, *Numerical modelling of nanoparticle deposition in the nasal cavity and the tracheobronchial airway.* Computer Methods in Biomechanics and Biomedical Engineering, 2011. **14**(7): p. 633-643.
6. Hindle, M. and P.W. Longest, *Evaluation of enhanced condensational growth (ECG) for controlled respiratory drug delivery in a mouth-throat and upper tracheobronchial model.* Pharmaceutical research, 2010. **27**(9): p. 1800-1811.
7. Chen, X., et al., *Numerical investigation of the interaction, transport and deposition of multicomponent droplets in a simple mouth-throat model.* Journal of Aerosol Science, 2017. **105**: p. 108-127.
8. Zhang, Z., et al., *Comparison of micro-and nano-size particle depositions in a human upper airway model.* Journal of aerosol science, 2005. **36**(2): p. 211-233.
9. Cheng, Y.-S., Y. Zhou, and B.T. Chen, *Particle deposition in a cast of human oral airways.* Aerosol Science & Technology, 1999. **31**(4): p. 286-300.
10. Cheng, K.-H., et al., *In vivo measurements of nasal airway dimensions and ultrafine aerosol deposition in the human nasal and oral airways.* Journal of Aerosol Science, 1996. **27**(5): p. 785-801.
11. Cheng, Y.-S., et al., *Diffusional deposition of ultrafine aerosols in a human nasal cast.* Journal of Aerosol Science, 1988. **19**(6): p. 741-751.
12. Cohen, B.S., R.G. Sussman, and M. Lippmann, *Ultrafine particle deposition in a human tracheobronchial cast.* Aerosol Science and Technology, 1990. **12**(4): p. 1082-1091.
13. Zhang, Z. and C. Kleinstreuer, *Airflow structures and nano-particle deposition in a human upper airway model.* Journal of computational physics, 2004. **198**(1): p. 178-210.
14. Longest, P.W. and J. Xi, *Effectiveness of direct Lagrangian tracking models for simulating nanoparticle deposition in the upper airways.* Aerosol Science and Technology, 2007. **41**(4): p. 380-397.
15. White, F.M., *Fluid mechanics. 5th.* Boston: McGraw-Hill Book Company, 2003.
16. Inthavong, K., J. Tu, and G. Ahmadi, *Computational modelling of gas-particle flows with different particle morphology in the human nasal cavity.* The Journal of Computational Multiphase Flows, 2009. **1**(1): p. 57-82.
17. Li, A. and G. Ahmadi, *Dispersion and deposition of spherical particles from point sources in a turbulent channel flow.* Aerosol science and technology, 1992. **16**(4): p. 209-226.
18. Saffman, P., *The lift on a small sphere in a slow shear flow.* Journal of fluid mechanics, 1965. **22**(02): p. 385-400.
19. Islam, M.S., et al., *Ultrafine Particle Transport and Deposition in a Large Scale 17-Generation Lung Model.* Journal of Biomechanics, 2017.
20. ICRP and I.C.o.R. Protection, *ICRP Publication 66: Human Respiratory Tract Model for Radiological Protection*. 1994: Elsevier Health Sciences.